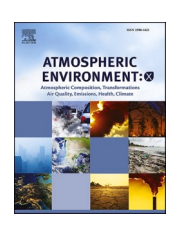
ELSEVIER

Contents lists available at ScienceDirect

Atmospheric Environment: X

journal homepage: www.journals.elsevier.com/atmospheric-environment-x





A modeling framework to assess fenceline monitoring and self-reported upset emissions of benzene from multiple oil refineries in Texas

Qi Li^{a,*}, Lauren Padilla^b, Tammy Thompson^c, Shuolin Xiao^a, Elizabeth J. Mohr^b, Xiaohe Zhou^d, Nino Kacharava^a, Yuanfeng Cui^a, Chenghao Wang^{e,f}

- ^a Cornell University, School of Civil and Environmental Engineering, 220 College Ave, Ithaca, 14850, NY, United States
- b Environmental Defense Fund. 18 Tremont St. Boston, 02108, MA. United States
- ^c Environmental Defense Fund, 2060 Broadway St, Boulder, 80302, CO, United States
- ^d Cornell University, Department of Computer Science, 107 Hoy Rd, Ithaca, 14850, NY, United States
- e School of Meteorology, University of Oklahoma, 120 David L. Boren Blvd., Norman, 73072, OK, United States
- f Department of Geography and Environmental Sustainability, University of Oklahoma, 100 E. Boyd Street, Norman, 73019, OK, United States

ARTICLE INFO

Keywords:

Fenceline monitoring

Hazardous atmospheric pollutant emissions

ABSTRACT

Benzene as one type of hazardous air pollutants (HAPs) is produced by industrial production processes and/or emitted during upset events caused by man-made or natural accidents. Although upset emissions of benzene can be a significant contributor to the total emission, it is still challenging to quantify. This study first develops a fast modeling framework using obstacle-resolving computational fluid dynamics modeling to compare the modeled within-facility-scale passive pollutant dispersion with the observed levels based on self-reported emissions for fourteen facilities in Texas, United States. Results of numerical simulations demonstrate that neglecting the obstacle effect can underpredict (overpredict) the near-(far-)field concentrations for a low source. For a source located above obstacles, underprediction occurs at all distances. The diagnostic framework is applied to 107 selfreported upset emission events for fourteen petroleum refineries in Texas from year 2019-2022. Considering different metrics across all events, it can be concluded that the modeled concentrations based on self-reported emissions likely underpredict the observed concentration increments. Depending on the possible source height, the median factor of underprediction ranges from 3 to 95 based on the average-plume metric. The agreement between model and observation is better for events characterized by high emission amounts and rates, which also correspond to high observed concentration increments. Overall, the research highlights the importance of considering obstacles and demonstrates the potential application of the current approach as an efficient diagnostic method for self-reported upset emissions using fenceline observations of HAPs.

1. Introduction

Benzene from the petroleum industry (Brief et al., 1980; Agency for Toxic Substances and Disease Registry, 2007) represents one type of hazardous atmospheric pollutants (HAPs). In particular, it is a global phenomenon that petroleum refineries release large amounts of benzene, contributing to elevated concentrations at facility fencelines (Jephcote and Mah, 2019; Kunstman et al., 2021), with upset emissions being a major contributor. According to the definition of upset air emissions (or upset emissions for brevity) (McCoy et al., 2010), they are "excess event emissions (duration usually less than 24-h) generated by unforeseen and/or sudden uncontrollable activities or malfunctions."

These excess event emissions are in contrast to the "routine" fugitive and stack emissions that are considered part of normal operations. Although unintended, upset emissions are not rare. They occur frequently in the petroleum industry and may include explosions, tank ruptures, compressor failures, flaring, and weather-triggered equipment failure.

As with many HAPs, benzene is harmful to human health even at low concentrations (Smith, 2010; Duarte-Davidson et al., 2001; Karakitsios et al., 2007; Bentayeb et al., 2015). For example, benzene is classified by the U.S. Environmental Protection Agency (U.S. Environmental Protection Agency National Center for Environmental Assessment, 2003) as a "known" human carcinogen for all routes of exposure including inhalation. There is no recommended safe level of exposure for benzene

E-mail address: ql56@cornell.edu (Q. Li).

 $^{^{\}ast}$ Corresponding author.

according to the World Health Organization (World Health Organization, 2019).

The occurrence of high benzene concentrations for communities living close to petroleum refinery facilities (Kunstman et al., 2021; Jephcote and Mah, 2019) poses challenges to environmental justice globally. For example, in an analysis across Europe of benzene exposures from the petrochemical industry, Jephcote et al. (Jephcote and Mah, 2019) found that the most polluting facilities tended to be located within financially disadvantaged regions and were associated with regional health disparities. Kunstman et al. (2021) found that more than 53,000 people live within 3 miles of one of the thirteen U.S. refineries that exceeded the $9 \mu g/m^3$ action level for the 12 month period ending on December 31, 2020. Of these people, an estimated 57% are people of color and 43% are living below the poverty line. Moreover, in the context of upset emission events in Texas, U.S., 4590 upset events releasing a variety of air pollutants, including benzene, have been reported (America, 2024), resulting in more than 135 million pounds of air pollutants.

However, challenges still persist in terms of quantifying upset emissions. For example, in the United States, they are more often calculated by engineering process conversion factors (Environmental Integrity Project, 2004). In Europe, the majority of petrochemical facilities calculate benzene emissions indirectly by chemical mass balance (43%) or other estimation methods (12%) (Jephcote and Mah, 2019). More importantly, the exposure and health risks of HAPs, such as benzene, are currently assessed by air quality models that implement emissions estimates without accounting for upset emissions. This omission is partly due to poor understanding of the contribution of upset emissions. Previous research applied detailed modeling to estimate emissions of benzene and other carbon aromatic compounds (Fang et al., 2016; Hu et al., 2015), but upset emissions were not explicitly accounted for. Nevertheless, the amount of emissions from upset events (Zirogiannis et al., 2018; Ozymy and Jarrell, 2011) can be substantial, as pointed out in (McCoy et al., 2010) in a regional study in Port Arthur, Texas. Their study by looking across 3900 events suggests that upset emissions from co-located refineries are equivalent to having an additional refinery within the region. There is existing evidence of benzene's significant impact on the regional ozone level (Murphy and Allen, 2005; Nam et al., 2008) and Hollingsworth (Hollingsworth et al., 2021) has demonstrated a link between excess emissions, ozone concentrations, and increased elderly mortality in Texas, U.S. Therefore, quantifying and characterizing the properties of upset emissions are first necessary steps to mitigate the negative repercussions of HAPs.

In fact, increasing availability of near-field fenceline monitoring data (e.g., the benzene fenceline monitoring program of the U.S. Environmental Protection Agency (EPA)) (Agency, 2024) and mobile measurement platforms (Caulton et al., 2018), provide new opportunities to better quantify facility-specific emissions of benzene and other HAPs more generally. Even though the EPA fenceline monitoring program only considered ground-level, persistent fugitive emissions, the passive samplers are theoretically able to capture signals of both upset (intermittent) and persistent emissions. The increasingly available fenceline monitoring data can be carefully examined to better understand the causes and properties of the upset emissions. They can also help to reconcile possible discrepancies or inconsistencies in the self-reported upset emissions across different facilities due to different methods of emission calculation. For example, it has been shown that causes or characteristics of the upset emissions lead to widely varied performance in facilities and reporting even for the same size facility (McCoy et al., 2010; Zirogiannis et al., 2018). A US EPA evaluation of data collected for a recent proposal to update national emission standards for synthetic organic chemical manufacturers (Bouchard et al., 2023) compared measured benzene fenceline concentrations with modeled concentrations based on reported emissions at 8 chemical manufacturing facilities, finding that average measured benzene concentrations were at least 2.7 and up to 56.6 times greater than average modeled concentrations.

Another recent detailed numerical modeling study for three refineries was conducted by Gray and Sahu (2023) using the American Meteorological Society/Environmental Protection Agency Regulatory Model (AERMOD). Importantly, they concluded that the self-reported emissions could be as much as 28-fold too low given the modeling results. However, it is well-known that obstacles, such as tanks, buildings, and stacks, present in the facility can affect the accuracy of AERMOD. For example, the down-wash module to account for building effect on dispersion has been included in AERMOD (Petersen et al., 2022). Other studies using monitoring data to quantify the emissions are based on regional-scale air quality models (Carmichael et al., 2003; Fang et al., 2016; Hu et al., 2015), but such approach is not applicable to the sub-kilometer scale problem involving individual facilities. A diagnostic framework to be applied broadly to multiple facilities to evaluate the potential discrepancy between reported upset emissions and those derived from fenceline monitoring data does not exist yet.

Therefore, this study aims to first develop an approach that can be applied to examine factors, such as presence of obstacles and upset emission height relative to obstacles, that influence the spatial distribution of non-reactive HAPs at the sub-kilometer scale relevant to fenceline monitoring. Secondly, the approach will be applied to fourteen sites in Texas to understand the potential discrepancy between the modeled and measured benzene concentration, using self-reported upset emission values.

This paper is organized as follows. Sec.2.1 describes the numerical model, which has been developed in our previous studies. Sec.2.2 introduces the self-reported upset emission dataset and the benzene fenceline measurement. Sec.2.3 explains the procedure for model observation comparison. Results and discussion are presented in Sec.3 and Sec.4.

2. Methodology

2.1. Large-eddy simulation coupled with Lagrangian stochastic particle models (LES-LSM)

A brief description of the LES-LSM approach is given here. Results have been published previously elsewhere for the local-scale dispersion in an urban environment (Wang et al., 2018a, 2018b). The LSM implemented in this paper is modified according to Thomson (1987) (Thomson, 1987). The original model derives a stochastic evolution equation for the subgrid-scale (SGS) velocity of a fluid parcel based on the local ensemble-mean velocity and velocity variances of the flow. Here, we replace the ensemble-mean velocity with the time-averaged LES-resolved velocity and calculate the velocity variances derived from the LES-resolved and SGS-modeled values. Based on those statistics, simulations of particle trajectories are then performed. With the pre-generated velocity and turbulence statistics, the LES-LSM framework has a low computational overhead that accounts for variations of the characteristics of emission sources, i.e., source locations and heights with respect to the obstacles. Evaluations of the code against wind-tunnel data for dispersion in an environment with building obstacles can be found in Wang et al. (2018b).

Here a database of concentration fields are created using the coupled framework of LES-LSM. The key assumption in the model is that a steady state condition is achieved for a constant emission rate. This assumption can be inappropriate under low mean wind speed and high horizontal velocity fluctuations (Qian and Venkatram, 2011). However, we checked that durations of all of upset emission events are longer than the advection time scale, which is computed as dimension of each facility divided by the mean wind speed. The steady-state assumption also facilitates comparison between modeled concentration with the fourteen-day averaged values registered by the fenceline monitors. Another assumption we made is that only neutral stability is considered here, which is a limitation of the current database. Previous studies such as a wind-tunnel measurement by Marucci and Carpentieri (2020) found

that concentration within the roughness sublayer can be up to three times lower in unstable stratification compared to neutral condition. Thus, assuming neutral condition leads to a higher modeled concentration, which favors the reported emissions (see more details in Sec.3.2). The roughness structures within the facilities are represented by arrays of cuboids with varying spacing and heights. These cuboids are highly idealized representations of the roughness structures in a real facility (i.e., tanks and stacks with coexisting pipes). According to the Toxics Release Inventory (TRI) 2020 dataset, majority of the stack heights are between 8 and 12 m, thus we consider two heights, 8 m and 16 m for the cuboids. The cuboids are spaced apart by 16 or 32 m to represent two spacing densities. For each value of the height and the spacing, we set up one simulation to represent the type of geometric configuration (so there are four configurations). Due to highly idealized assumption about the geometry, to understand how results are influenced by presence of obstacles, we also perform simulations without presence of any obstacles. Three different wind directions are simulated (See Fig. 1a) due to symmetry of the cuboid arrays. The flow simulated by LES is forced with a constant pressure gradient $\frac{\partial p}{\partial z_f}$. The velocity field obtained is nondimensionalized by the surface friction velocity $u_{\mbox{\tiny \ast}}$ of 1 m/s and it is ensured that $\rho u_*^2 = \frac{\partial p}{\partial z_f}$, where ρ is the density of air, here being set as a constant. For each geometric configuration, locations of the sources are systematically varied (See Fig. 1a). Specifically, three groups of the source height z_s for low (high) cuboid height is considered, namely, 'low', where z_s ranges from 2 to 4 m (4–8 m); 'medium', where z_s ranges from 4 to 6 m (8–12 m); and 'high', where z_s ranges from 8 to 10 m (16-20 m) (See Fig. 1b). Such choice is motivated by setting up cases to understand how emissions located below the mean obstacle height or above affects the dispersion. Hence, for different types of upset emissions due to various causes, i.e., flaring, tank malfunctions, startups, etc., some insight into their expected detailed dispersion behavior can be learned. For computational efficiency, location of the emitted particles in the LSM runs are randomly selected from a neighborhood of $3 \times 3 \times 3$ grid points, which are equivalent to $3m \times 3m \times 3m$. The final database contains concentration fields of 120 different scenarios (4 underlying geometries \times 10 different source locations \times 3 different wind directions). The full database of results is used for subsequent analysis to compare with the fenceline monitoring data. Note that as shown in the top-down view of the source locations in Fig. 1, only three possible locations for low and medium z_s are obtained and four possible locations

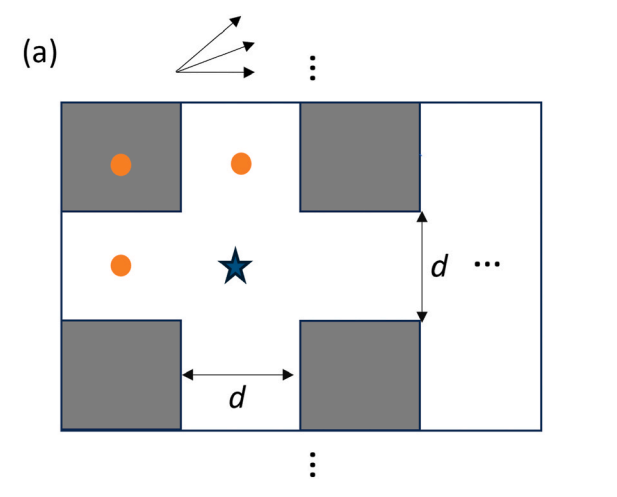
for z_s are obtained, thus in total 10 different source locations.

2.2. Reported upset emissions and fenceline monitoring data

The reported upset emissions in TCEQ's (Texas Commission on Environmental Quality) Air Emission Report Database from individual oil refineries from year 2019–2022 are analyzed. We selected those refineries where corresponding fenceline monitoring stations were set up. A total of fourteen refineries are identified. The reported emission dataset contains information crucial for the analysis described in Sec.2.3, which includes the emission duration (Du), total emitted amount (M), the reported start (T_s), and end (T_e) times of the incidents. The Supplementary Material contains information about statistics of these emission characteristics from the fourteen refineries (See Fig. S5).

The fenceline monitoring data are from the benzene fenceline monitoring program of the Environmental Protection Agency (2024) between Jan 01, 2019 to Jun 22, 2022. An overview of the program purpose and separate analysis of the fenceline monitoring data are provided in Sec. 2 in the Supplementary Material. Here we describe how we derive an observed concentration increment associated with upsets for comparison to the equivalent concentration increment predicted by the model.

The observed two-week averaged $C_{14,o}$ ($\mu g/m^3$), with the subscript indicating observation and subscript '14' indicating two-week period, when a reported upset emission event occurred during that two-week period is used for further analysis. Note that non-upset emissions, such as permit allowable fugitive and stack emissions, upsets that did not meet the reporting threshold (10 lbs for benzene (T. C. on Environmental Quality, 2020) and Table 3 in (Archives, 2023)), and emissions from other near-field sources can also affect $C_{14,0}$ and they are assumed to lead to a background benzene concentration $C_{bg,o}$. Thus, $C_{14,}$ $_{o}$ is affected by both $C_{bg,o}$ and the upset emissions that lead to a two week-averaged concentration increment $C'_{14,o}$. We tested the sensitivity of the concentration increment derived from observation to three different methods of estimating $C_{bg,o}$. The first method takes the minimum monitor concentration among all $C_{14,o}$ values; the second method takes the average of periods without reported upset emissions and discounting two-weeks after any reported upset emission; the third method applies a three-month moving average to $C_{14,0}$. It is noted that these three methods to quantify $C_{bg,o}$ are not ideal as one would have measured the upwind concentrations during every upset emission event.



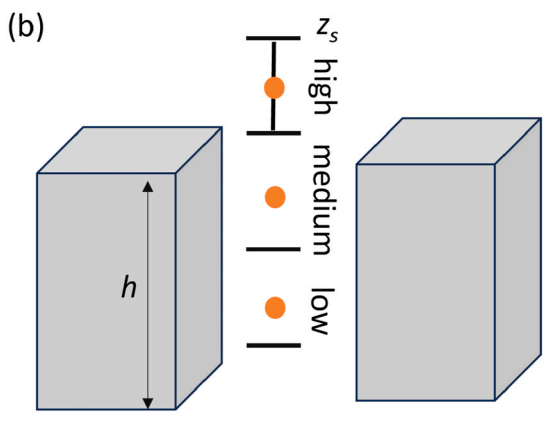


Fig. 1. (a) Sketch of an overlook of the obstacles, which are cuboids of height h with base of 100 m \times 100 m and are spaced d apart. h=8 m or 16 m and d=100 m or 200 m. The orange filled circles and the blue star indicate positions of the emissions relative to the obstacles. The blue star indicates location of the source shown in Fig. 2. Three wind directions of 0° , 22.5°, and 45° relative to obstacles were considered. (b) Illustration of the three groups of the source heights, namely, low, medium, and high, ranging from 0.25 to 0.5 h, 0.5–0.75 h, and 1–1.25 h, for one of the prescribed positions. Note that only when source height is high, an emission source is located directly above the obstacle. (For interpretation of the references to color in this figure legend, the reader is referred to the Web version of this article.)

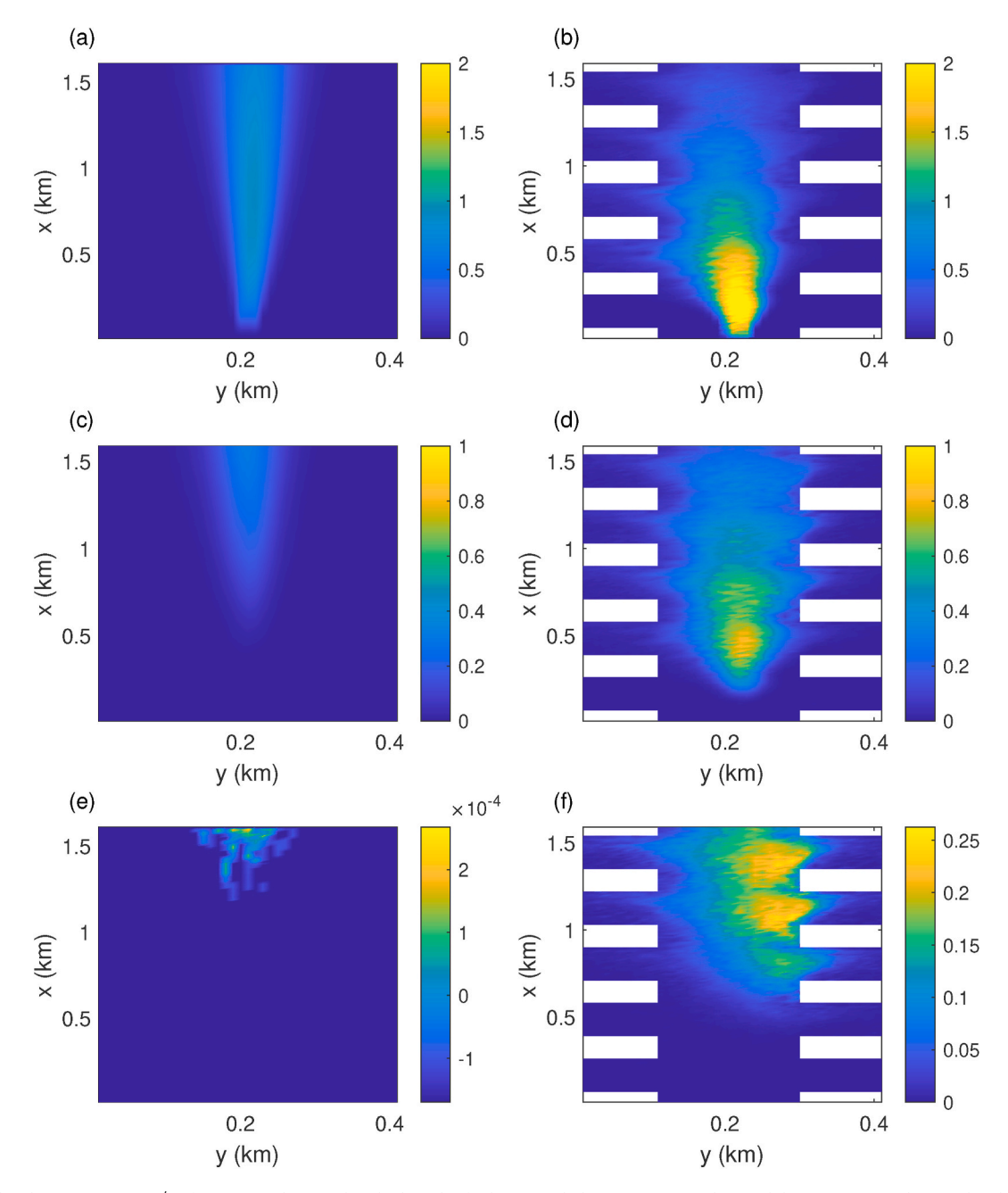


Fig. 2. Normalized concentrations C'_{LES} for cases without and with obstacles for horizontal plane at z=2 m. The wind direction is zero degree, the obstacle geometry is sparse-low. The obstacles, i.e., the "white-bars" are $100 \text{ m} \times 100 \text{ m}$ and the gap between, d, is 200 m in this example. The planar location of the source is indicated by the blue star in Fig. 1a; the top, middle, to bottom rows show cases with source heights corresponding to low, medium, and high as indicated in Fig. 1b. (a), (c), (e): C'_{LES} for cases without obstacles with source heights z_s low, medium and high. (b), (d), (f): C'_{LES} for case with sparse-low obstacles with source heights z_s low, medium and high. (For interpretation of the references to color in this figure legend, the reader is referred to the Web version of this article.)

Current methods might result in low bias in $C'_{14,o}$. This implies that if the modeled concentration (See Sec.2.2) is lower than such conservative estimate of $C'_{14,o}$, it will further confirm the likelihood of under-reporting of upset emissions. Furthermore, we showed that the conclusions are not sensitive to different definitions of $C_{bg,o}$ (See Tables S4 and S5 in the Supplementary Material). The *second* method of calculating the background concentration is used for subsequent analyses. We compare the measured $C'_{14,o}$ with the modeled equivalent, $C'_{14,m}$, where the subscript 'm' denotes m odel, as computed by

$$C'_{14,m} = C'_m \times \frac{(T_e - T_s)}{Du_{14}},$$
 (1)

where C_m' is the average concentration increment during the upset period defined by T_s and T_e , the event start and end times, respectively, and the constant Du_{14} is the two-week period matching the observed sample duration, i.e., 336 h (14 days × 24 h/day). For reported events with duration that spans across more than one consecutive measurement period, a similar method can be applied for each two-week period. For example, $C_{14,m}1$ and $C_{14,m}2$ can be derived in the first and second two-week periods for comparison to the $C_{14,0}$ in respective periods. Note that Eq. (1) is equivalent to assuming that in the time not impacted by the emission event, i.e., $Du_{14} - (T_e - T_s)$, there is zero concentration increment.

2.3. Comparing modeled concentrations with observations

For each of the upset emission event in a given facility, the exact location of the emission remains uncertain. However, given the perimeter-siting of the fenceline monitors, it is a reasonable assumption to make that there exist some monitors located downwind of the emission that are likely to capture the plume due to upset emissions. Therefore, even though the exact location of the emission relative to the downwind fenceline monitors is unknown, by exploring a large number of possible relative positions between emission source and monitors in the simulated concentration dataset, some insight into how a facility's local obstacles impact the concentration spatial distributions can be gained. If we further assume that at least one of the fenceline monitors is located within the plumes of any emission, then concentrations of the simulated plumes that arise from the reported emissions can be compared with the observed fenceline monitoring concentrations (when adjusted for the background concentrations) across all the facilities for all reported upset emission events. We emphasize here that our goal here is not to precisely determine the upset emission strength nor its locations for each emission event in a given facility. Nevertheless, accuracy of reported upset emissions can be evaluated by exploring a large range of possible relative locations between the emission and the monitor locations. Implications of the assumptions and limitations of the analysis method are further discussed in Sec.4.4.

A method similar to (Caulton et al., 2018) is implemented to scale the modeled concentration by the reported emission rate and the wind speed in the nearest station to every facility during the reported upset emission event. Because all LES-LSM runs are non-dimensionalized, the modeled output C_{LES} needs to be scaled to represent the actual field conditions for a given emission event. The procedure of scaling the modeled concentration is briefly described here. The LES-LSM non-dimensional and dimensionalized (denoted with a superscript D) outputs can be related by Eq. (2), which can be inferred from the stationary advection–diffusion equation or by analogy to the scaling of a Gaussian model:

$$C'_{m} = \frac{Q^{D}}{Q_{LES}} \times \frac{U_{LES}}{U^{D}} \times C'_{LES}, \tag{2}$$

where C_m is the dimensional concentration given the reported emission rate Q^D for a single upset emission event; Q_{LES} is the emission rate set as 1 g/s in the LES-LSM simulation. The non-dimensional modeled wind speed in LES, U_{LES} is divided by the dimensional U^D , which is the wind speed from nearest meteorological stations to the facility. Because onsite measurement of wind speed is not available, the station data are seen as a background wind speed. U_{LES} is taken to be the free-stream velocity in the atmospheric surface layer at twice of the obstacle height.

3. Results

Despite the highly idealized setup of the geometric configuration, the effect of local obstacles on dispersion can be quantified by analyzing the spatial distributions and vertical profiles of the concentration (Sec.3.1). Sec.3.2 then compares the concentration obtained from reported upset emissions with the observed ones.

3.1. Effects of obstacles and source locations to the observed concentrations

To understand the effect of local obstacles on dispersion, the comparison between non-dimensional modeled concentration increment obtained with an emission rate of 1 g/s, C_{LES} , is shown in Fig. 2 for horizontal slices being taken at z=2m. Three different source heights z_s are considered and location of the source is in between arrays of obstacles as indicated by the cross in Fig. 1a. Pronounced cross-wind dispersion in the case with obstacles is observed for all three source heights z_s . In addition, the obstacles perturb the atmospheric surface

layer and create stronger vertical spread of the plume and thus the case with highest z_s (Fig. 2f) shows much higher magnitude near surface compared to the corresponding one without the obstacle (Fig. 2e). The lateral displacement of C_{LES} for lower z_s is higher closer to the source in cases with obstacles than cases without. This is consistent with a reduced streamwise mean advective transport due to drag force exerted by the obstacles on the ambient flow (Davidson et al., 1996). Similarly, as shown in Fig. S1 for horizontal slices of concentration at z = 10 m, in cases of low z_s, the cross-wind dispersion and vertical spread of the plumes are more significant with obstacles. As explained in (Davidson et al., 1996), when large bluff-body-type obstacles are present, two mechanisms simultaneously affect the behavior of a plume, namely the divergence (convergence) of the streamline and the change of the nature of turbulence induced by the obstacles. The faster spread of the plume in cases with obstacles are due to the interplay of these two mechanisms. Note that the obstacles considered are highly idealized and they are not meant to reflect the details of any particular facility. However, the above described mechanism can still affect the dispersion in a real facility and qualitative conclusions can be drawn here by comparing the case with and without obstacles. This may imply that in a real facilities, the near-ground monitors (i.e., located from 1.5 m-3 m according to the standard procedure) that are located closer to the source will likely be able to capture the plume, as compared to the case without obstacles.

Effects of the obstacle can be analyzed by considering non-dimensionalized height z/h, where h is the mean obstacle height. Even though h differs for different facilities and obstacles within facilities have non-uniform heights, the vertical profiles can be non-dimensionalized by h, such that some generalizable trends independent of h can be analyzed.

Fig. 3 shows the vertical profile of cross-wind plume-width averaged concentration as a function of height scaled by h for increasing downstream distance x_L away from the source are at $x_L = h$, 10h, 100h. The plume-width for different x_L is defined as locations where the concentration falls to 1% of the centerline value. The vertical spread of the plume is consistent with the discussions above as obstacles intensify mixing and deflect the plumes upwards. This is especially the case for larger x_L (i.e., the bottom row in Fig. 3). In general, if the monitoring stations are located 1.5 m-3 m from the ground and h in a facility is likely to be higher than 3 m, then focusing on $\langle C'_{LES} \rangle_{\nu}$ (i.e., $\langle \rangle_{\nu}$ denoting plume-width-averaging) for z/h < 1 generates some useful insight into the measurement strategies and estimation of the emission rate can be inferred from these vertical profiles. For lower source positions, where $z_s = 0.2h$ and 0.5h, omitting obstacles would underestimate the nearfield concentrations for $h < x_L < 10h$; whereas the effect would be overestimating the far-field concentrations for $x_L \approx 100h$. Such trend can be more clearly seen by the percentage difference between $\langle C_{LES}' \rangle_{v}$ with and without obstacles at z/h = 0.5, where monitors are most likely to be below such height (See figure titles in Fig. 3). This implies that if obstacles are not accounted for when inversely modeling emissions, the emission source strength will be overestimated (underestimated) for near (far) sources, as Q^D in Eq. (2) is proportional to $\frac{C_{14.0}}{C_{model}}$, where C_{model} is the concentration from any model, such as the standard Gaussian plume model. In addition, if the source is located at $z_s = 1.2h$ and the downwind monitors are close to the source (i.e. $x_L = h$ and 10h), then it is unlikely that the emission will be detected regardless of whether obstacles are present or not (Fig.s 3b,c) because the plume passes above the monitors. For such reason, we did not simulate cases of source height that could represent the stack leakages, e.g., z = 2h, as they are likely not being able to be picked up by the fenceline monitors located within 100h downwind under neutral stability. When the distance x_L between emission location and the monitoring stations is 100 h, which is considered as a 'far' source location (i.e., Fig. 3 last row), the enhanced vertical spread of the plumes in cases with obstacles implies that the near-surface monitoring stations should be quite likely to detect such a emission event. It is also interesting to note that in some of the fenceline monitor

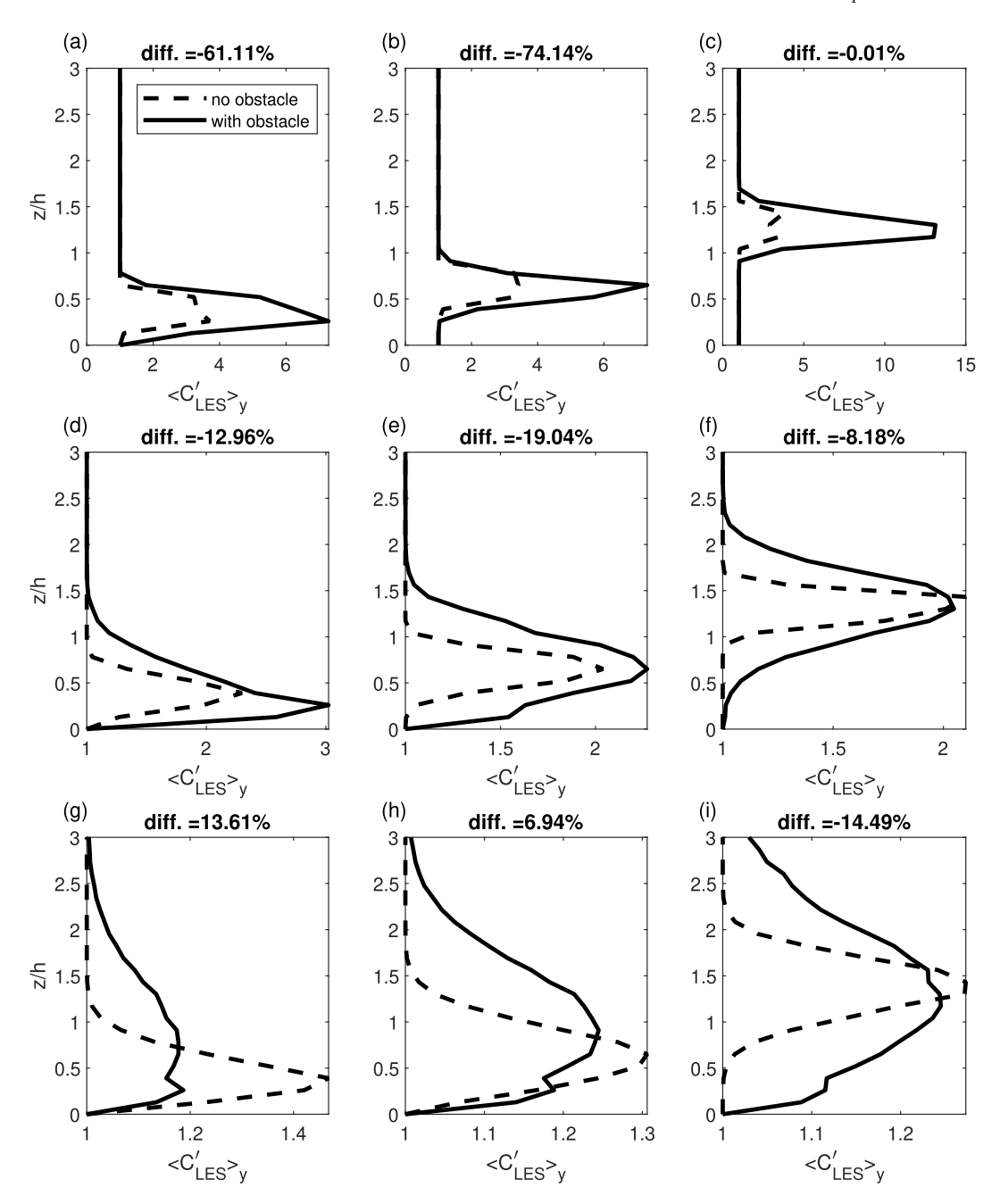


Fig. 3. Vertical profile of cross-wind plume-width averaged normalized concentrations $\langle C'_{LES} \rangle_y$ as a function of height scaled by h for increasing downstream distance x_L away from the source. Left column (a), (d), (g): source height z_s low $(0.2h < z_s \le 0.5h)$; middle column (b), (e), (h): z_s medium $(0.5h < z_s \le 0.8h)$; right column (c), (f), (i): z_s high $(0.8 \ h < z_s \le 1.2h)$. Dotted line corresponds to case without obstacles; solid line corresponds to the configuration of sparse, low obstacles. The plumewidth for different x_L is defined as locations where the concentration falls to 1% of the centerline value. Top row (a)–(c): distance $x_L = h$ from the source location; middle row (d)–(f): $x_L = 10 \ h$; bottom row (g)–(i): $x_L = 100 \ h$ 'diff.' in the figure title refers to percentage difference of $\langle C'_{LES} \rangle_y$ between cases with and without obstacles.

data, a single monitor shows a high anomaly whereas in some other data, adjacent monitor stations all show high anomalies often accompanied by a distinct maximum in one of the monitors. These different characteristics of the observations are likely caused by two reasons: firstly, the variation in mean wind direction moves the centroid of the plume across multiple sampling locations; secondly, different scenarios that correspond to different x_L and z_s result in different plume widths. Due to large variations of the concentration profiles across the scenarios, it is challenging for fenceline monitors often located all at a single height to infer the locations of the emission by pinpointing the exact values of x_L and z_s .

The effects of different geometries of the obstacles are analyzed in Fig. 4. If observation is close to the source and exactly located downwind, sparsely space obstacles give rise to the highest concentration, as a result of stronger streamwise advective transport. Location of the concentration maxima is consistent with their respective z_s values. For larger x_L values (Fig.s 4 d-i), the tall obstacle cases (i.e., purple lines) show a more diffuse profile than the low obstacle cases (i.e., black lines). Together with the profiles for cases without obstacles in Fig. 3, this is consistent with the streamline divergence due to presence of obstacles of increasing h (Davidson et al., 1996). Apart from the turbulent entrainment, the mean flows dominantly influence the plume growth, as the

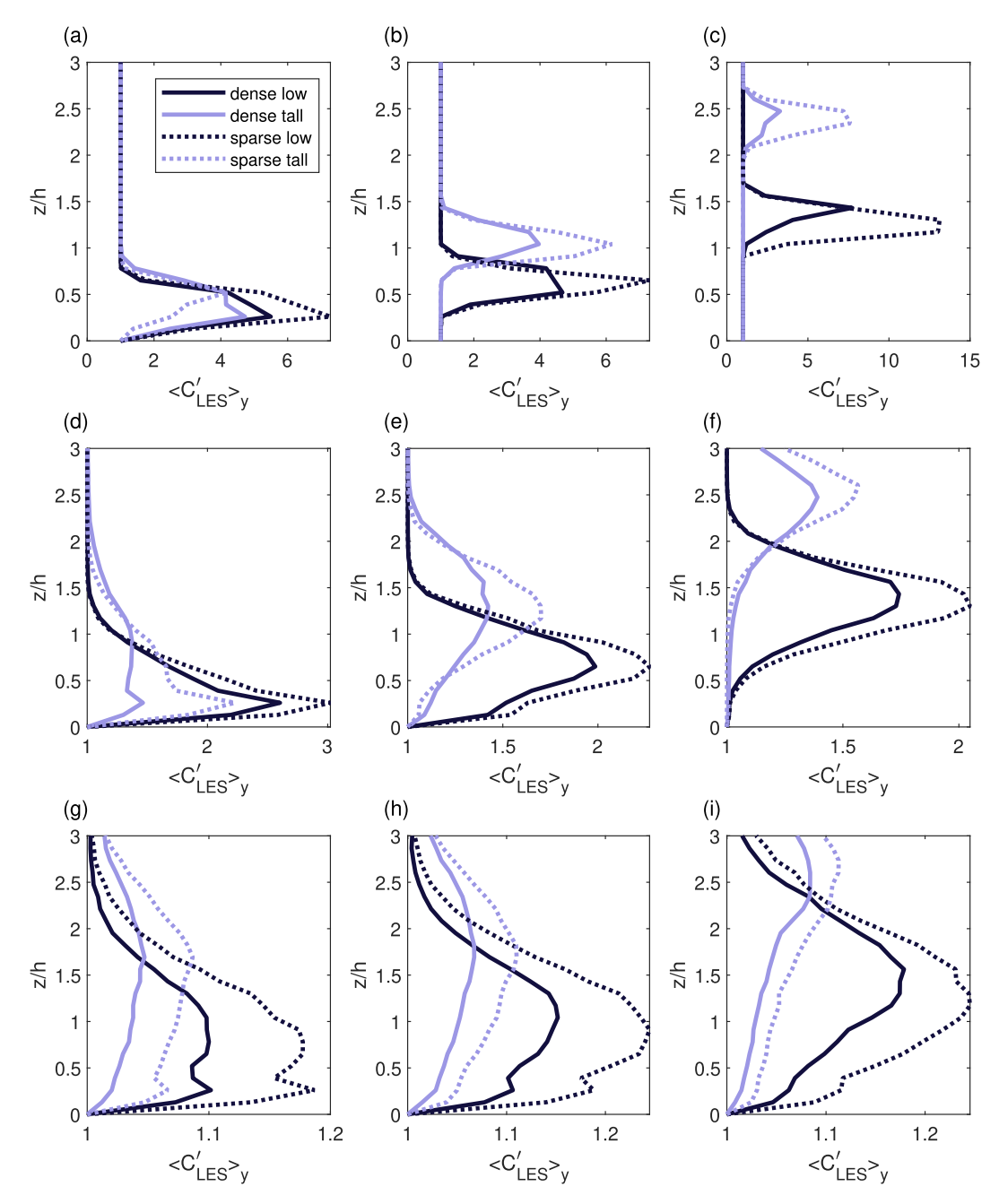


Fig. 4. Profiles of normalized concentrations $\langle C_{LES} \rangle_y$ for four different types of obstacles. Left column (a), (d), (g): source height z_s low $(0.2h < z_s \le 0.5h)$; middle column (b), (e), (h): z_s medium $(0.5h < z_s \le 0.8h)$; right column (c), (f), (i): z_s high $(0.8h < z_s \le 1.2h)$. Top row (a)–(c): distance $x_L = h$ from the source location; middle row (d)–(f): $x_L = 10h$; bottom row (g)–(i): $x_L = 10h$. Columns from left to right indicate different source heights z_s .

cross-wind spread of the plumes across cases with different geometries are similar as shown in the cross-wind profiles in the Supplementary Material (See Fig.s S2 and S3).

3.2. Comparison of reported upset emissions data and fenceline monitoring data

As explained in Sec.2.3, the comparison between model results and measurements can be carried out by considering the average distance between the emission location and the perimeter of the facility with a monitor located downwind at fenceline position (x_f, y_f, z_f) in a Cartesian coordinate. Note that this problem has two degrees of freedom, which are the relative height and the relative planar distance between the source and the monitor, denoted as $z_s - z_f$ and x_L , respectively. Here we

estimate x_L by taking the minimum distance between each monitor and the centroid of the facility. With a fixed estimate x_L , the problem is reduced to only one degree of freedom. For a particular facility, we consider $C_{14,m}(\overline{x_L})$ for three different groups of z_s ranging from low $(0.2h < z_s \le 0.5h)$, medium $(0.5h < z_s \le 0.8h)$, to high $(0.8 \ h < z_s \le 1.2h)$, where $\overline{x_L}$ corresponds to the respective value in Table S2. The maximum value in each of the z_s groups for all $C_{14,m}(\overline{x_L})$ in a given facility is denoted as $Max[C_{14,m}']$, which is then compared with $C_{14,o}$. Considering $Max[C_{14,m}']$ ensures that we always pick the highest possible concentration from the modeled dataset, given computed $\overline{x_L}$ for a specific facility, such that we deliberately avoid selecting low modeled concentrations a priori when comparing with the observed ones. In addition, in some cases, multiple monitors could show elevated concentrations due to the

plume's crosswind structure, the range of concentration maximum given multiple monitors in one facility is estimated using the standard bootstrap method and the lower and upper bounds are $C^l_{o,max}$ and $C^u_{o,max}$, respectively.

Fig. 5 shows the comparison between $Max[C'_{14,m}]$ (i.e., the abscissa) and $C_{o.max}^{u,\prime}$ $(C_{o.max}^{l,\prime})$ (i.e., the ordinate) for three groups of z_s . Most of the points lie above the one-to-one line, indicating that if an upset emission is located $\overline{x_L}$ away from a monitor exactly downwind, most of the observed concentrations are still larger than the maximum of modeled concentrations. As z_s changes from low to high, $Max[C'_{14m}]$ taken at the monitor height $z_m = 3$ m decreases, which is consistent with results based on analysis in Sec.3.1 that the near-ground concentration for high source location is lower than that for lower source locations. However, the variations with z_s are not substantial compared to the inherent variability of $Max[C'_{14,m}]$ across all the emission events. Another notable difference between $Max[C_{14,m}']$ and $C_{o,max}^{l,\prime}$ $(C_{o,max}^{u,\prime})$ is that the observed values span across approximately two orders of magnitude. However, the variability of the modeled values span across about five orders of magnitude. Due to the large spread of $Max[C_{14,m}']$, we show the 75th percentile and median values of $\frac{C'_{o,max}^{l}}{Max[C'_{14,m}]}$ and $\frac{C'_{o,max}^{l}}{Max[C'_{14,m}]}$ in Table 1. The 75th percentile and median values differ by about a factor of 10, indicating individual events with substantial variation of M, Q, and Du might affect $C'_{14,m}$, which will be analyzed subsequently.

To quantify the variations across all upset emission events among the fourteen facilities, the ratio between $Max[C'_{14,m}]$ and $C'_{0,max}$ is shown in Fig. 6. The values of $Max[C'_{14,m}]/C'^{,l}_{0,max}$ are colored by log(M) (See Fig. 6) and log(Q) (See Fig. S7 in the Supplementary Material). The results for

low z_s are shown here and similar to the variation across increasing z_s shown in Fig. 5, $Max[C'_{14,m}]/C'^{l}_{o,max}$ decreases with increasing z_s (results not shown). Upset emission events with larger magnitudes of M and Q as indicated by the color scale generally correspond to higher values of $Max[C'_{14,m}]/C'^{l}_{o,max}$, especially for larger log(M), evidenced by most facilities, especially in 'ExBay', 'VaE', 'ExBae', and 'Tot'. There are two reasons why the model and measurements may agree better for events with larger emission magnitudes and rates. One reason could be due to the nature of the fenceline measurements: a 14-day passive sampler will smooth over upset emission events with short duration and small magnitude due to its low sampling rate, making their signal more difficult to distinguish from background routine emissions, which are known to be present. Another reason could be due to larger events that preferentially occur at higher release points beyond high z_s , such as tall stacks, which lead to a low concentration registered by fenceline monitors due to higher elevations of the plume.

Despite the estimate of $\overline{x_L}$ favoring higher modeled concentration, uncertainty in our knowledge of x_L and z_s relative to location of the monitors can be addressed by defining two metrics pertaining to the entire plume. The first metric η is defined as the fraction of modeled plume concentration $C'_{14,m}$ that is below $C^l_{o,max}$. The second metric is $\frac{< C'_{o,max}>}{< C'_{14,m}>}$, which is defined as the ratio between the average modeled plume concentration and mean of the upper and lower bounds of the estimated maximum of observed concentrations, i.e., $1/2(C^l_{o,max}+C^u_{o,max})=< C'_{o,max}>$. For both metrics, the plume is defined as the upper quartile of a horizontal slice of $C'_{14,m}$ at each modeling height from the surface to 8 m (i.e., within the mean obstacle height) extending to the

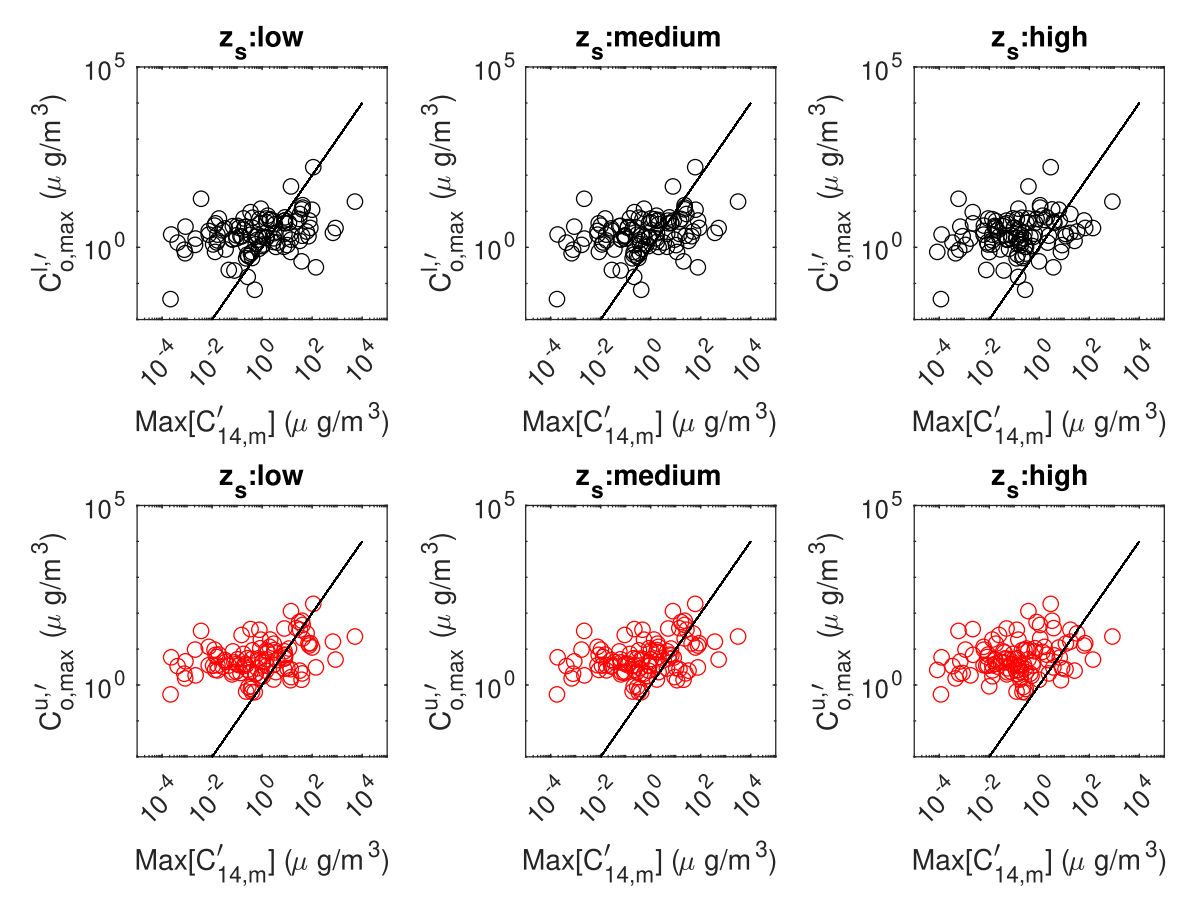


Fig. 5. Comparison between modeled concentration located $\overline{x_L}$ distance downwind of the source for and the observed maximum concentrations. (a)–(c): The upper bound of observed concentration for each emission event at a given facility, $C_{o,max}^{u'}$ versus the maximum value among all $C_{14,m}(\overline{x_L})$ for a given facility, $Max[C_{14,m}]$; (d)–(e): same as (a)–(c) except the ordinate being the lower bound $C_{o,max}^{l'}$.

Table 1 Statistics of $\frac{C_{o,max}^{',l}}{Max[C_{14.m}]}$, $\frac{C_{o,max}^{',u}}{Max[C_{14.m}]}$, $\frac{C_{o,max}^{',u}}{Max[C_{14.m}]}$, $\frac{C_{o,max}^{',u}}{Amx[C_{14.m}]}$, and $\frac{C_{o,max}^{',u}}{C_{14.m}}$ across all upset emission events (107 in total) for three groups of different values of z_s .

z_s	$rac{C_{o,max}^{\prime \perp}}{Max[C_{14,m}^{\prime}]}$		$\frac{C_{o.max}^{\prime,u}}{\textit{Max}[C_{14,m}]}$		η (%)		$\frac{< C_{o,max}>}{< C_{14,m}>}$	
	75th percentile	median	75th percentile	median	mean	median	mean	median
Low	26.4	2.48	51.6	4.87	84.1	98.1	156	3.02
Mid.	28.1	3.20	83.0	7.50	87.8	99.74	415	8.05
High	128	15.2	283	37.4	94.6	100	4900	95.0

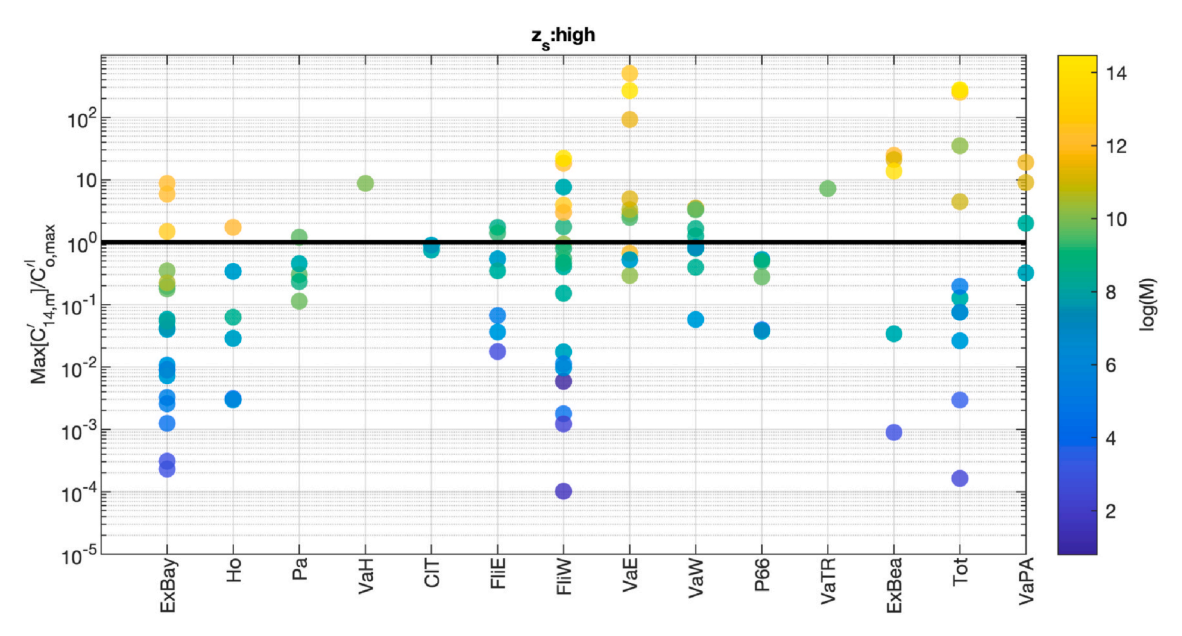


Fig. 6. Ratio between modeled concentration located $\overline{x_L}$ distance downwind of the source and the observed maximum concentrations for fourteen facilities. The points are colored by the quantity of upset emissions and the color is in log scale. (For interpretation of the references to color in this figure legend, the reader is referred to the Web version of this article.)

downwind distance of 1.92 km (i.e., the total domain length). Sensitivity analysis of the definition of plume is performed by varying the percentile values and vertical height, which do not change conclusion of the results. These two metrics defined with respect to the plume can be seen as encompassing a wide range of possible upset emission locations, which would have included scenarios with actual relative distance even smaller than the estimate of $\overline{x_L}$ above.

The mean and median values of η and $\frac{<C_{o,max}>}{< C_{14,m}>}$ for all upset emission events are shown in Table 1. For half of events, η is close to 100%, as shown by the large median values. Similar trend with respect to z_s can also be seen from mean and median values of $\frac{<C_{o,max}>}{< C_{14,m}>}$. Despite uncertainty in the upset emission locations relative to monitors, these results suggest that, applying the reported emission rate, there is high probability that the corresponding model prediction, $C_{14,m}$, underestimates the observed value at any receptor distance and source height.

Examining the variation in η and $\frac{<C_{o,max}>}{< C_{14,m}>}$ across different upset emission characteristics in Table 2 shows that both are negatively correlated with the emission rate Q. A similar negative correlation with M can also be found (results not shown). However, there is not a clear negative correlation between η ($\frac{<C_{o,max}>}{< C_{14,m}>}$) and duration Du. Such trend indicates that for events with high M and moderately long Du, which correspond to events with high Q, the modeled and observed concentrations tend to agree more closely with each other. The values of $\frac{<C_{o,max}>}{< C_{14,m}>}$ averaged for the two upper quartiles of Q(M) is 85 (171) times of that

Table 2 Statistics of η , and $\frac{< C_{o,max} >}{< C_{14,m} >}$ averaged over events grouped according to quartiles of Q for three groups of different values of z_s .

z_s	η (%)				$\frac{< C_{o,max}>}{< C_{14,m}>}$			
Q	Q1	Q2	Q3	Q4	Q1	Q2	Q3	Q4
Low Mid. High	99.9 99.9 100	92.9 94.8 96.2	85.4 89.7 97.01	69.6 75.5 89.2	895 2386 28165	73 197 2326	9.0 23.9 282	2.4 6.4 75

averaged for the two lower quartiles, indicating a even more prominent under-reporting for events with small Q and M. Nevertheless, even for high-impact events of larger Q and M, large uncertainty in reporting M still can exist. More research needs to be done across the facilities regarding their general practice of reporting the upset events in terms of estimating M and Du.

4. Discussion

4.1. The effects of including obstacles on modeling concentrations and estimating emissions

Compared to the control case without obstacles, presence of obstacles leads to concentration enhancement closer to the source due to decreased mean transport in the downwind direction. This is especially

relevant for sources located below the mean obstacle height. On the other hand, arrays of obstacles also increase turbulent mixing. In particular, pollutants emitted from sources located above the mean obstacle height can be efficiently entrained below the obstacle level at a relatively shorter downwind distance from the source compared to cases without obstacles. These results imply that fenceline monitors at 1.5–3 m above the ground and located at a 500 m-3000 m (depending on size of the facility) downwind of possible emission sources can detect the plumes due to upset emissions either close to them or located above the obstacles. Results here imply that omitting obstacles generally leads to lower downwind, near-surface modeled concentrations. The larger the facility, farther the fenceline from the source, and the higher the source release, the more underprediction resulting from omitting the obstacle effect will be. Therefore, apart from the source being low (below the mean obstacles height) and far ($x_L = 100h$), neglecting obstacles in most cases would introduce a low bias in the model predictions of concentrations. This finding also corroborates with results in Pirhalla et al. (2021), where they reported that EPA's AERMOD using Gaussian dispersion modeling neglecting effects of obstacles underestimates the concentrations, especially at the far field. The evidence suggests that results from Gaussian dispersion models without accounting for effects of the obstacles, such as often used as the basis of regulatory risk assessments, lead to biased comparison to real world observations at the near-ground level.

As already mentioned in Sec.3.1, the effects of obstacles can affect the estimation of emission using an inverse modeling approach. Since the estimated emission Q^D is proportional to $\frac{C'_{14.0}}{C_{model}}$, where C_{model} is usually inferred from inverse-modeling approach given some known emission rate Q_{model} . Thus, an underprediction of C_{model} means the overestimation of Q^D for most cases if neglecting the obstacle effect. In other words, neglecting obstacles, one would erroneously estimate a given observed concentration was caused by a larger emission event than actually occurred.

4.2. Implications for the U.S. EPA fenceline monitoring program

It is important to note that a statistically significant positive correlation (correlation coefficient = 0.31 with p-value of 0.01) between monitored concentration increment and reported emission rate is found, as shown in Fig. S6 in the Supplementary Material. This suggests that the fenceline concentrations and upset emissions reported by individual facilities are likely to be consistent, at least qualitatively, with the occurrence of upset events. However, modeling results in Sec.3.1 show that substantial under-reporting can still be quite prevalent after accounting for the uncertainties in source locations and obstacle configurations, which are consistent with previous studies (Bouchard et al., 2023; Gray and Sahu, 2023). Also, as the fenceline monitors record both non-upset and upset events, the statistically significant correlation between them strongly hints at the importance of upset emissions in total emissions, which are typically neglected in air quality modeling. Future studies could evaluate the correlation between the concentration increment and the routine emissions, if data become available.

In addition, the modeled and observed concentrations are in closer agreement when the reported events are characterized by high emission amount and high emission rate, which also means the high anomalies of observed concentrations. All these evidences indicate that if an upset event involved high emissions and tend to happen for longer than a few hours (but not longer than one week), they are likely to be more accurately reported in terms of the total emission amount. It can be speculated that high anomalies of fenceline monitored concentrations might trigger a more thorough investigation of incidences leading to such upset emissions. Thus, it is also of future interest to understand the role of fenceline monitoring results in shaping facilities' practice or protocol of reporting these events.

4.3. Recommendations of monitoring and reporting system for HAPs

The proposed diagnostic framework can be extended to other HAPs, where the chemical lifetime is longer than their mixing time in the sub-kilometer scale. The framework is also transferable to other industrial sources of air pollution, in which similar fenceline monitoring and upset emission reporting systems similar to that in Texas have been set up. Based on results in this study, we make the following general recommendations regarding the monitoring and reporting system for HAPs.

- Expanding fenceline monitoring is a necessary first step to apply a
 diagnostic framework similar to the proposed method to assess the
 potential under-reporting more widely. The model underprediction
 for benzene upset emissions demonstrated here makes a strong case
 for the need to expand fenceline monitoring.
- If more frequent reporting of routine emissions becomes available, (i.
 e., rather than the annual-average, which is typical among emission
 inventories), the current diagnostic framework can be applied to
 fenceline monitoring results.
- 3. For upset emissions and routine emissions, more detailed reporting on the location of the emission source, especially the estimated source height and distance to perimeter, would improve the precision of emission quantity and rate estimates derived using the current framework.
- 4. It is expected that measurement-based quantification of upset emissions and routine emissions would be possible, provided onsite meteorological condition such as wind speed and direction, together with monitors at more than a single height become available. Then, the measurement can be combined with inverse modeling method that is appropriate for this sub-kilometer-scale problem for emission estimation.

With improved monitoring and reporting systems for HAPs, the spatiotemporal resolution of the emission inventories can be further improved, facilitating better comparisons with observations and further improvements to emission estimates.

4.4. Implications of assumptions and limitations of current study

Here we summarize how assumptions and limitations of this study affect the analysis results, especially pertaining to the comparison between model and observation.

Firstly, wind directions at the local refinery during duration of upset emissions may not be accurately represented by the weather stations. A global cross check of wind direction indicates that at least one fenceline monitor showing elevated values was located downwind using the wind direction data for majority of the upset emission events. Therefore, it is quite likely that signals from upset emissions have been captured by the fenceline monitors.

Secondly, this study is limited by not being able to distinguish upset and non-upset emissions due to data availability. However, the fenceline monitors show signals of all emission types. We applied three methods (See Sec.2.2) to calculate background concentration $C_{\rm bg,o}$ and to disentangle the signal due to the upset events. The higher concentration increment during reported upset emission events shown in Table S3 in the Supplementary Material confirms that it is possible to distinguish upset emissions, despite larger uncertainty if the events are characterized by short duration and small magnitude. Such uncertainty may drive the lower end of the comparative result that currently spans orders of magnitude.

Thirdly, one of the assumptions is that the plume centerline is aligned with locations of the fenceline monitors for the entirety of emission, such that a maximum overlap exists. However, this is unlikely to be the case because of gaps between the fenceline monitors and unsteady wind directions causing plume meandering. To alleviate this problem, we created a statistical estimate of the maximum of the con-

centration increment (See Sec.3.2). Note that the non-overlapping effect will result in lower observed concentration increment, which even further confirms under-reporting if $C_{o.max}' > Max[C_{14.m}']$.

Fourthly, this study is limited by only considering neutral stability in the generated database. In unstable conditions, concentration within the roughness sublayer is lower than that in neutral stability due to increased vertical mixing (Marucci and Carpentieri, 2020), vice versa for stable conditions. However, considering the operations of facilities releasing waste heat and high sensible heat flux during daytime, unstable condition might occur more frequently. An estimation of the stability parameter z/L based on a sensible heat flux of 500 W/m² and surface friction velocity of 0.5 m/s, z/L ranges from 0.13 to 0.44 for z=3-10 m. Thus, the modeled neutral concentration potentially has a high bias, but this will not change the main conclusion of the paper regarding potential under-reporting.

5. Conclusion

In this study, we applied a computational fluid dynamics modeling approach using LES coupled with LSM to understand the effects of obstacles on the dispersion of a passive tracer. Assuming a constant continuously released emission source, a dataset of three dimensional concentration field consisting of 120 different scenarios (i.e., variable obstacle heights, arrangements, wind directions, and source locations) was generated. Despite the idealized setup of the simulations, these conclusions are expected to be generalizable to fenceline monitors around the facilities at a spatial scale below 2 km. Then, this dataset is scaled by the reported benzene upset emissions in fourteen facilities, where fenceline monitors were installed to record the two-week-averaged benzene concentrations.

Even though the exact locations of the benzene upset emissions are unknown, the generated concentration fields correspond to a large number of possible relative locations between emission and monitors downwind, which enable comparisons between the modeled and the observed concentrations. As inferring the exact source locations from the two-week-averaged monitoring data can be challenging, we considered the modeled concentration increments due to upset emissions at a minimum source distance $\overline{x_L}$ from a downwind fenceline monitor. Two metrics η and $\frac{<C_{0,max}>}{<C_{1,4m}>}$ are also computed to compare the modeled and observed concentrations. Using the reported emission rate and assuming the source is located at distance $\overline{x_L}$ away from a downwind fenceline monitor, majority of the events show underprediction, where the median values of $\frac{<C_{0,max}>}{<C_{0,1,4m}>}$ across all considered events ranges from 3 to 95 (See Table 1) depending on the source height.

In light of the two study aims, a few key take-away points that can be generalized beyond the benzene fenceline data considered in this study are summarized below.

- Results from the obstacle-resolving LES-LSM suggest that effects of obstacles need to be considered for modeling ground-level concentrations of non-reactive HAPs, especially for fenceline dispersion studies at the kilometer to sub-kilometer scale.
- 2. The source height relative to the obstacles and ground-level (i.e., 1.5–3 m fenceline monitors) measurement locations in terms of downwind distance from the source location are important factors controlling the concentration. Omitting obstacles in modeling would underestimate concentrations at all distances for near-ground measurements if the source height is above the obstacles.
- 3. The obstacle-resolving LES-LSM can be applied to generate a dataset with variable obstacle configurations, wind directions, and atmospheric stability (to be considered in future studies). By considering appropriate metrics of evaluation, the dataset can be applied to have a fast, first-order evaluation of the accuracy of self-reported emissions across multiple facilities.

CRediT authorship contribution statement

Qi Li: Writing – review & editing, Writing – original draft, Supervision, Project administration, Methodology, Investigation, Funding acquisition, Formal analysis, Conceptualization. Lauren Padilla: Writing – review & editing, Writing – original draft, Resources, Project administration, Methodology, Investigation, Conceptualization. Tammy Thompson: Writing – review & editing, Writing – original draft, Resources, Project administration, Methodology, Investigation, Conceptualization. Shuolin Xiao: Validation, Software, Methodology, Investigation, Formal analysis, Data curation. Elizabeth J. Mohr: Writing – review & editing, Writing – original draft, Resources, Investigation. Xiaohe Zhou: Software, Methodology, Investigation, Formal analysis. Nino Kacharava: Writing – original draft, Visualization, Investigation, Formal analysis. Yuanfeng Cui: Validation, Methodology, Investigation. Chenghao Wang: Writing – review & editing, Validation, Software, Methodology.

Declaration of competing interest

The authors declare that they have no known competing financial interests or personal relationships that could have appeared to influence the work reported in this paper.

Data availability

Data will be made available on request.

Acknowledgements

This work was supported by gifts to Environmental Defense Fund and Cornell Atkinson Center for Sustainability from the David and Patricia Atkinson Foundation and by Bloomberg Philanthropies (Grant ID 2023-126011).

Appendix A. Supplementary data

Supplementary data to this article can be found online at https://doi.org/10.1016/j.aeaoa.2024.100281.

References

- Agency, E.P., 2024. Fenceline Monitoring Program Overview. Environmental Protection Agency. URL: https://awsedap.epa.gov/public/extensions/Fenceline_Monitoring/Fenceline_Monitoring.html?sheet=background. (Accessed 13 May 2024).
- Agency for Toxic Substances and Disease Registry, 2007. Toxicological Profile for Benzene. Technical Report. U.S. Department of Health and Human Services. URL: https://www.atsdr.cdc.gov/toxprofiles/tp3.pdf.
- America, E., 2024. Illegal air pollution in Texas. Environment America. URL: https://e nvironmentamerica.org/texas/resources/illegal-air-pollution-in-texas/. (Accessed 13 May 2024).
- Archives, N., 2023. Code of Federal Regulations, Title 40, Chapter I, Subchapter J, Part 302, Technical Report.
- Bentayeb, M., Wagner, V., Stempfelet, M., Zins, M., Goldberg, M., Pascal, M., Larrieu, S., Beaudeau, P., Cassadou, S., Eilstein, D., Filleul, L., Le Tertre, A., Medina, S., Pascal, L., Prouvost, H., Quénel, P., Zeghnoun, A., Lefranc, A., 2015. Association between long-term exposure to air pollution and mortality in France: a 25-year follow-up study. Environ. Int. 85, 5–14. https://doi.org/10.1016/j.envint.2015.08.006. URL: https://www.sciencedirect.com/science/article/pii/S0160412015300349.
- Bouchard, A., Cantoni, M., Lavoie, T., 2023. Technical Memorandum: Clean Air Act Section 112(d)(6) Technology Review for Fenceline Monitoring Located in the SOCMI Source Category that Are Associated with Processes Subject to HON and for Fenceline Monitoring that Are Associated with Processes Subject to Group I Polymers and Resins NESHAP. Technical Report. U.S. Environmental Protection Agency. EPA Docket No. EPA-HQ-OAR-2022-0730. https://www.regulations.gov/document/EPA-HO-OAR-2022-0730-0091.
- Brief, R.S., Lyncha, J., Bernath, T., Scala, R.A., 1980. Benzene in the workplace. Am. Ind. Hyg. Assoc. J. 41, 616–623. https://doi.org/10.1080/15298668091425392, 10.1080/15298668091425392, publisher: Taylor & Francis _eprint.
- Carmichael, G.R., Tang, Y., Kurata, G., Uno, I., Streets, D.G., Thongboonchoo, N., Woo, J.-H., Guttikunda, S., White, A., Wang, T., Blake, D.R., Atlas, E., Fried, A., Potter, B., Avery, M.A., Sachse, G.W., Sandholm, S.T., Kondo, Y., Talbot, R.W.,

- Bandy, A., Thorton, D., Clarke, A.D., 2003. Evaluating regional emission estimates using the TRACE-P observations. J. Geophys. Res. Atmos. 108 https://doi.org/10.1029/2002JD003116,eprint. URL: https://onlinelibrary.wiley.com/doi/abs/10.1029/2002JD003116 https://onlinelibrary.wiley.com/doi/pdf/10.1029/2002JD003116.
- Caulton, D.R., Li, Q., Bou-Zeid, E., Fitts, J.P., Golston, L.M., Pan, D., Lu, J., Lane, H.M., Buchholz, B., Guo, X., et al., 2018. Quantifying uncertainties from mobilelaboratory-derived emissions of well pads using inverse Gaussian methods. Atmos. Chem. Phys. 18, 15145–15168.
- Davidson, M., Snyder, W., Lawson Jr., R., Hunt, J., 1996. Wind tunnel simulations of plume dispersion through groups of obstacles. Atmos. Environ. 30, 3715–3731.
- Duarte-Davidson, R., Courage, C., Rushton, L., Levy, L., 2001. Benzene in the environment: an assessment of the potential risks to the health of the population. Occup. Environ. Med. 58, 2–13. URL: https://oem.bmj.com/content/58/1/2, 10.1136/oem.58.1.2, publisher: BMJ Publishing Group Ltd Section: Review.
- Environmental Integrity Project, 2004. Gaming the system: how off-the-books industrial upset emissions cheat the public out of clean air. Technical Report. URL: https://environmentalintegrity.org/reports/gaming-the-system/.
- Fang, X., Shao, M., Stohl, A., Zhang, Q., Zheng, J., Guo, H., Wang, C., Wang, M., Ou, J., Thompson, R.L., Prinn, R.G., 2016. Top-down estimates of benzene and toluene emissions in the Pearl River Delta and Hong Kong, China. Atmos. Chem. Phys. 16, 3369–3382. URL: https://acp.copernicus.org/articles/16/3369/2016/.doi:10.5194/acp-16-3369-2016,publisher:CopernicusGmbH.
- Gray, A.G., Sahu, R., 2023. New study: refineries under-reported benzene emissions by as much as 28-fold. URL: https://news.oilandgaswatch.org/post/new-study-refineriesunder-reported-benzene-emissions-by-as-much-as-28-fold.
- Hollingsworth, A.J., Konisky, D.M., Zirogiannis, N., 2021. The health consequences of excess emissions: evidence from Texas. J. Environ. Econ. Manag. 108, 102449 https://doi.org/10.1016/j.jeem.2021.102449. URL: https://linkinghub.elsevier. com/retrieve/pii/S0095069621000322.
- Hu, L., Millet, D.B., Baasandorj, M., Griffis, T.J., Travis, K.R., Tessum, C.W., Marshall, J. D., Reinhart, W.F., Mikoviny, T., Müller, M., Wisthaler, A., Graus, M., Warneke, C., de Gouw, J., 2015. Emissions of C6–C8 aromatic compounds in the United States: constraints from tall tower and aircraft measurements. J. Geophys. Res. Atmos. 120, 826–842. https://doi.org/10.1002/2014JD022627_eprint. URL: https://onlinelibrary.wiley.com/doi/pdf/10.1002/2014JD022627 https://onlinelibrary.wiley.com/doi/pdf/10.1002/2014JD022627.
- Jephcote, C., Mah, A., 2019. Regional inequalities in benzene exposures across the European petrochemical industry: a Bayesian multilevel modelling approach. Environ. Int. 132, 104812 https://doi.org/10.1016/j.envint.2019.05.006. URL: https://www.ncbi.nlm.nih.gov/pmc/articles/PMC68857433/.
- Karakitsios, S.P., Delis, V.K., Kassomenos, P.A., Pilidis, G.A., 2007. Contribution to ambient benzene concentrations in the vicinity of petrol stations: estimation of the associated health risk. Atmos. Environ. 41, 1889–1902.
- Kunstman, B., Schaeffer, E., Shaykevich, A., 2021. Environmental Justice and Refinery Pollution: Benzene Monitoring Around Oil Refineries Showed More Communities at Risk in 2020, Technical Report. Environmental Integrity Project. URL: https://e nvironmentalintegrity.org/wp-content/uploads/2021/04/Benzene-report-4.28.21. pdf.

- Marucci, D., Carpentieri, M., 2020. Dispersion in an array of buildings in stable and convective atmospheric conditions. Atmos. Environ. 222, 117100.
- McCoy, B.J., Fischbeck, P.S., Gerard, D., 2010. How big is big? how often is often? characterizing Texas petroleum refining upset air emissions. Atmos. Environ. 44, 4230–4239
- Murphy, C.F., Allen, D.T., 2005. Hydrocarbon emissions from industrial release events in the houston-galveston area and their impact on ozone formation. Atmos. Environ. 39, 3785–3798. https://doi.org/10.1016/j.atmosenv.2005.02.051,cited.by:98. URL: https://www.scopus.com/inward/record.uri?eid=2-s2.0-20744435768&doi=10.10 16%2fj.atmosenv.2005.02.051&partnerID=40&md5=a6f971e564bb2f057445 2a43792e27cb.
- Nam, J., Webster, M., Kimura, Y., Jeffries, H., Vizuete, W., Allen, D.T., 2008. Reductions in ozone concentrations due to controls on variability in industrial flare emissions in houston, Texas. Atmos. Environ. 42, 4198–4211. URL: https://www.scopus.com/inward/record.uri?eid=2-s2.0-43849110971&doi=10.1016%2fj.atmosenv.2008.01.035&partnerID=40&md5=e754aca0aea408088877b05980b2d328, 10.1016/j. atmosenv.2008.01.035, cited by: 24; All Open Access, Green Open Access.
- Ozymy, J., Jarrell, M.L., 2011. Upset over air pollution: analyzing upset event emissions at petroleum refineries. Rev. Pol. Res. 28, 365–382. URL: https://onlinelibrary.wiley.com/doi/abs/10.1111/j.1541-1338.2011.00502.x. doi:10.1111/j.1541-1338.2011.00502.x. eprint.
- Petersen, R.L., Paumier, J.O., Guerra, S.A., 2022. Development, evaluation, and implementation of building downwash and plume rise enhancements in aermod. J. Air Waste Manag. Assoc. 72, 1423–1441.
- Pirhalla, M., Heist, D., Perry, S., Tang, W., Brouwer, L., 2021. Simulations of dispersion through an irregular urban building array. Atmos. Environ. 258, 118500.
- Qian, W., Venkatram, A., 2011. Performance of steady-state dispersion models under low wind-speed conditions. Boundary-Layer Meteorol. 138, 475–491.
- Smith, M.T., 2010. Advances in understanding benzene health effects and susceptibility. Annu. Rev. Publ. Health 31, 133–148. https://doi.org/10.1146/annurev. publhealth.012809.103646. URL: https://www.annualreviews.org/doi/10.1146/annurev.publhealth.012809.103646.
- T. C. on Environmental Quality, 2020. Texas Administrative Code, Title 30, Chapter 101, Technical Report. Texas Office of the Secretary of the State.
- Thomson, D., 1987. Criteria for the selection of stochastic models of particle trajectories in turbulent flows. J. Fluid Mech. 180, 529–556.
- U.S. Environmental Protection Agency National Center for Environmental Assessment, 2003. Integrated risk information system (IRIS) chemical assessment summary for benzene; CASRN 71-43-2. Technical Report. https://iris.epa.gov/static/pd fs/0276 summary.pdf.
- Wang, C., Wang, Z.-H., Yang, J., Li, Q., 2018a. A backward-Lagrangian-stochastic footprint model for the urban environment. Boundary-Layer Meteorol. 168, 59–80.
- Wang, C., Li, Q., Wang, Z.-H., 2018b. Quantifying the impact of urban trees on passive pollutant dispersion using a coupled large-eddy simulation–Lagrangian stochastic model. Build. Environ. 145, 33–49.
- World Health Organization, 2019. Exposure to benzene: a major public health concern. URL: https://www.who.int/publications/i/item/WHO-CED-PHE-EPE-19.4.2.
- Zirogiannis, N., Hollingsworth, A.J., Konisky, D.M., 2018. Understanding excess emissions from industrial facilities: evidence from Texas. Environ. Sci. Technol. 52, 2482–2490.